International Journal of Applied Earth Observations and Geoinformation 110 (2022) 102813

Contents lists available at ScienceDirect

International Journal of Applied Earth Observations and Geoinformation

journal homepage: www.elsevier.com/locate/jag

Estimation of mean dominant height using NAIP digital aerial photogrammetry and lidar over mixed deciduous forest in the southeastern USA

Elizabeth M. Prior [a,*], Valerie A. Thomas [b], Randolph H. Wynne [b]

[a] Dept. of Biological Systems Engineering, Virginia Tech, Blacksburg, VA 24061, USA
[b] Dept. of Forest Resources and Environmental Conservation, Virginia Tech, Blacksburg, VA 24061, USA

ARTICLE INFO

Keywords:
Forestry
Lidar
Airborne laser scanning
Digital aerial photogrammetry
Mean dominant height

ABSTRACT

In the absence of complete lidar coverage, digital surface models (DSMs) and point clouds produced from the United States Department of Agriculture National Agriculture Imagery Program (NAIP) are increasingly being analyzed for quality and application feasibility. This study compared canopy heights derived from NAIP DSMs (10 m) and point clouds to those derived from lidar data collected over Mountain Lake Biological Station and the Great Smoky Mountains Twin Creeks Site by the National Ecological Observatory Network (NEON) Airborne Observation Platform for 62 mixed deciduous tree plots. Mean dominant height (MDH) was estimated using lidar and the NAIP products using the 90th percentile of heights in a given plot as the independent variable for both the lidar- and NAIP-derived point clouds. The dependent variable was field-measured MDH, calculated using the four tallest trees for each 0.04-hectare plot based on the NEON woody vegetation structure dataset. All data (field and remotely sensed) were collected in 2018. Using maximum likelihood spatial error model for all analyses, the NAIP DSM (10 m resolution) resulted in a strong relationship with MDH (coefficient of determination (R^2) = 0.90, standard error (SE) = 1.71 m). However, the 90th percentiles of heights derived from the point clouds were better at estimating MDH than was the comparatively coarse resolution DSM (NAIP point clouds: $R^2 = 0.94$, $SE = 1.40$ m; lidar: $R^2 = 0.95$, $SE = 1.29$ m, respectively) and are strongly correlated to each other ($R^2 = 0.99$, $SE = 0.68$ m). The main limitation of the NAIP datasets was found to be where shadowing occurred due to steep terrain in the Great Smoky Mountain site. These areas resulted in erroneously high vegetation heights. Mean dominant heights estimated using NAIP DSMs and point clouds are thus comparable to those estimated using lidar data in these closed-canopy temperate deciduous forests where shadowing from steep terrain is not present. The utility of both the NAIP-derived 10 m DSM and the point clouds for estimating tree heights paves the way for statewide mapping of heights over the deciduous forests in Tennessee, Virginia, and possibly beyond.

1. Introduction

Remote sensing has progressively found a foothold in forestry due to its nondestructive multitemporal ability to assess vertical structure and function over large expanses. Three-dimensional structural data, commonly collected through active remote sensing techniques, are robust in both precision and accuracy, with the most prevalent being light detection and ranging (lidar) also known as aerial laser scanning. Unfortunately, this technology does not come without limitations. Monetary cost and required power consumption have limited the extent of the Earth that is covered by lidar as well as the potential for repeated datasets. Due to these limitations, determining how other remote sensing methods compare to lidar has become an active research topic within the forestry community (Goodbody et al., 2019).

A viable alternative to lidar is digital aerial photogrammetry (DAP) point clouds, also known as photogrammetric point clouds or phodar. DAP point clouds are created by imagery that is commonly collected in either a frame-based or pushbroom (linear array) configuration. Frame-based collection relies on overlapping images to create the point cloud. Pushbroom collection consists of sensor arrays at various angles used for continuous scanning, where overlap and coverage are gained from the forward scanning motion (Strunk et al., 2020). Resolution of collected

* Corresponding author.
E-mail addresses: eprior@vt.edu (E.M. Prior), thomasv@vt.edu (V.A. Thomas), wynne@vt.edu (R.H. Wynne).

https://doi.org/10.1016/j.jag.2022.102813
Received 1 November 2021; Received in revised form 9 March 2022; Accepted 6 May 2022
Available online 19 May 2022

imagery can vary widely, though image resolution has not been shown to greatly skew forest parameter results (Bohlin et al., 2012; Gobakken et al., 2015; Nurminen et al., 2013; Strunk et al., 2020). Strunk et al. (2020) did find that frame-based DAP point clouds slightly outperformed pushbroom DAP point clouds with less canopy irregularity captured, though it was concluded that both were still capable of reporting high-quality forest measurements at a plot level.

Numerous studies have shown that DAP point clouds are capable of measuring fundamental forest parameters relevant to forest health monitoring and assessment (Bohlin et al., 2012; Immitzer et al., 2016; Järnstedt et al., 2012; Pearse et al., 2018; Pitt et al., 2014; Puliti et al., 2015; St-Onge et al., 2008; Strunk et al., 2019, 2020; Vastaranta et al., 2014, 2014; White et al., 2015). Accurate and frequent measurements of such parameters (height, Lorey's height, basal area, diameter) is paramount for the health and safety of ecosystem services, protection against fire and better management practices. The main appeal to DAP point clouds is that the image collection process is a common remote sensing practice that is much cheaper than lidar, up to one third the cost of lidar (Goodbody et al., 2019, 2019; Michez et al., 2020; Navarro et al., 2020; Ritz et al., 2021; White et al., 2015). One operational DAP program is the United States Department of Agriculture (USDA) National Agriculture Imagery Program (NAIP).

Since 2003, NAIP has collected red, green and blue (RGB) aerial imagery of the United States (US) during leaf-on every year. This imagery has a one meter ground sample distance and has a horizontal accuracy that matches within six meters of photo-identifiable ground control points (USDA, 2011). This started as a five-year cycle and transitioned to a three-year cycle in 2009 (Ritz et al., 2021). The data has improved to have a 4 m horizontal accuracy since 2016 and 40 cm to 60 cm resolution starting in 2018. In 2007, some states also began to collect near infrared (NIR) data. For the 2018 acquisition, the US Forest Service (USFS) and other federal agencies paid for additional processing of the NAIP data to extract point clouds and 10 m digital surface models (DSM) (NAIP, 2018). The states included Connecticut, Delaware, Maine, Maryland, Massachusetts, North Carolina, New Hampshire, Rhode Island, Vermont, Virginia, Tennessee and West Virginia. The point clouds and DSM data were only processed in 2018. Future funding for processing is uncertain, but could enable repeated height measurements for those states.

Limited research has been done using NAIP data. Most have paired NAIP multispectral imagery with other forms of remote sensing (Hartfield et al., 2011; Hogland et al., 2018; Ma et al., 2017; Maxwell et al., 2014; Samiappan et al., 2019) or solely used NAIP imagery for classification purposes (Basu et al., 2015; Davies et al., 2010; Liknes et al., 2010). There are limited studies investigating estimation of forest parameters from NAIP point clouds; existing studies focus on using NAIP in Washington, US for large forest area estimation (Strunk et al., 2019), comparison of NAIP point clouds to lidar and other DAP collection methods and resolutions (Strunk et al., 2020) and using NAIP point clouds to measure loblolly pine planation heights (Ritz et al., 2021). If NAIP point clouds were continuously measured, there is great potential to have multitemporal vegetation structural data for the entirety of the US. One limitation to the NAIP DAP data is that acquisition can occur months apart, resulting in adjacent flight lines being collected at different dates and potentially at different sun angles, all of which could greatly affect the accuracy of the DAP data. Further research would need to be conducted in order to investigate how drastic this effect would be, how much of the NAIP data would be affected by this, and if there are any remediative techniques that could be implemented.

DAP point clouds require high-resolution digital elevation models (DEM) for point cloud normalization and canopy height models (CHM) derivation. This need is continuously being addressed by the US Geological Survey (USGS) 3D Elevation Program (3DEP), which aims to provide free DEMs of the entire US by 2023 (Lukas and Baez, 2021). From these free data sources comes the possibility of reduced forest inventory costs along with a multitude of other ecosystem services and dynamics monitoring and assessment. The potential for this type of data has already been realized in other countries, most notably in Switzerland where a multitemporal study of 35 years was conducted for above ground biomass dynamics assessment using DAP point clouds that were systematically collected from the Federal Office of Topography (Price et al., 2020).

Our study aims to exhibit the potential that NAIP point clouds have to offer as an alternative to lidar for deciduous forest height measurements. The objective of this study is to determine whether the NAIP DAP point clouds and DSM datasets can accurately estimate mean dominant tree height for plots in mixed eastern deciduous forests. This was accomplished by comparing 2018 NAIP DSM and DAP point clouds to 2018 lidar and tree field measurements all collected by the at National Ecological Observatory Network (NEON) at Mountain Lake Biological Field Station (MLBS), Virginia, US and Great Smoky Mountains National Park Twin Creeks site (GRSM), Tennessee, US. MLBS is classified as mixed forest, being primarily dominated by maples and oaks, while GRSM consists of mixed deciduous trees while having primarily coniferous trees at higher altitudes. These classifications are important since forest parameters, such as site index, have been successfully inferred through remote sensing for loblolly pine plantations (Gopalakrishnan et al., 2019), but not yet for small areas of mixed and deciduous forests. Establishing relationships between remotely sensed data and forest parameters has the potential to increase sustainable land management and aid in monitoring and assessment for restoration purposes. If successful, the future of NAIP data could allow for the establishment of long-term point cloud datasets that could be applied to land management practices and provide alternative strategies for forest inventory data collection.

2. Materials and methods

2.1. Study areas

MLBS is located in Mountain Lake Wilderness Area within Jefferson National Forest (37.375654°, −80.522140°). The site is within the Appalachian Mountains of southwest Virginia on the eastern continental divide at elevations between 1,150 m to 1,319 m. Characteristic of the Valley and Ridge physiographic province, MLBS has narrow mountains consisting of Rosehill sandstone cliffs and Ordovician Reedsville Shale with Tuscarora outcroppings (Mills, 1988; Schultz et al., 1986; Wilbur et al., 2021). Soils are acidic infertile sandy loam, typically either Lily-Bailegap series complex, Cotaco Loam or Fluvaquents (Wilbur et al., 2021). The annual mean temperature is around 8.3° C with 146 days from early May to October typically being without frost. Snowfall is variable from year to year, while most rainfall occurs from April to October with a yearly average of 887 mm (Wilbur et al., 2021). Tree species tend to vary depending on the rock type, soils, moisture level, aspect and topography, with eastern white pine (*Pinus strobus*) occurring in mostly sandy areas, while north-facing concave hills have yellow birch (*Betula alleghaniensis*), striped maple (*Acer pensylvanicum*) and in moister areas rosebay rhododendron (*Rhododendron maximum*) (Mills, 1988; Wilbur et al., 2021). South-facing concave hills tend to be drier, having basswood (*Tilia*), sugar maple (*Acer saccharum*), oak (*Quercus*) and buckeye (*Aesculus*) (Mills, 1988). Convex hills are dominated by oaks (*Quercus*) and hickories (*Carya*). Extremely moist areas tend to have eastern hemlock (*Tsuga canadensis*) with red spruce (*Picea rubens*) occurring at higher elevations (Mills, 1988).

From historic logging and mountain pastures in the 18th century, only 1% of the MLBS forests are older than 150 years. MLBS was established in 1930 by University of Virginia's biology department as a teaching and research facility. MLBS joined NEON in 2015, and reports a multitude of data. Currently, the northern section is owned by the USFS and is managed for *Quercus alba*, timber harvesting and recreational hunting. The southern section is on a 50-year renewable lease held by University of Virginia.

GRSM is located in the Great Smoky Mountains National Park within the blue ridge physiographic province (35.68896°, −83.50195°). The park was established in 1934 and is the most visited national park in the US. The park encompasses the Great Smoky Mountains, a subset of the southern Appalachian Mountains, along the border of east Tennessee and North Carolina. The park is almost all forested with about a third consisting of old growth forest. Elevation ranges from 267 m to 2,025 m with the topography generally regarded as rugged (Jenkins, 2007). The geology and subsequently the soils are highly variable, with meta-quartzite bedrock along with slates and mafic rock and limestone (Jenkins, 2007; Southworth et al., 2004). Rainfall typically varies from 140 cm to 200 cm, depending on elevation, with a mean temperature of 13.1° C. The park has long been recognized for its biological importance through its designations as an International Biosphere Reserve and a World Heritage Site, as well as being recognized as the North American center for vascular plant diversity, easily comprising over 1300 native plant species (Jenkins, 2007). This recognition and native plant tally is ongoing with the All Taxa Biodiversity Inventory (Sharkey, 2001).

For this study, ten tree plots are located in the Great Smoky National Park at the Twin Creeks Site (Fig. 1). Jenkins et al. (2007) notes that the Twin Creeks area has been historically disturbed by settlement and logging, and is considered low to mid elevation secondary forest (Jenkins, 2007). The NEON tree plots for this site largely consist of black gum (*Nyssa sylvatica*), carolina silverbell (*Halesia carolina*), chestnut oak (*Quercus montana*), eastern hemlock (*Tsuga canadensis*), pitch pine (*Pinus rigida*), red maple (*Acer rubrum*), scarlet oak (*Quercus coccinea*), sourwood (*Oxydendrum arboreum*), and tulip popular (*Liriodendron tulipifera*) (NEON, 2020a). The Twin Creeks Science and Education Center began in 2007 and acts as a research station for visiting scientists and houses natural history collections for the park. GRSM also joined NEON in 2015. The two sites are relatively representative of the larger Appalachian region, with most of the species commonly occurring throughout this region and a range of elevations represented from the plots. Additionally, NEON classifies both of them as being representative of the Appalachians and Cumberland Plateau.

2.2. Dataset descriptions

2.2.1. Field data

The primary field measurements for trees at NEON sites include height, crown diameter and diameter at breast height (DBH) with the goal of enabling biomass and productivity estimates, along with calibration and validation for NEON remote sensing products (NEON, 2020a). These measurements are typically conducted annually for trees with a DBH greater than 10 cm (3.94 in.). For all data provided by NEON, they ensure quality assurance and quality control via their data quality program, and their airborne remote sensing data quality technical working group and their data standards technical working group.

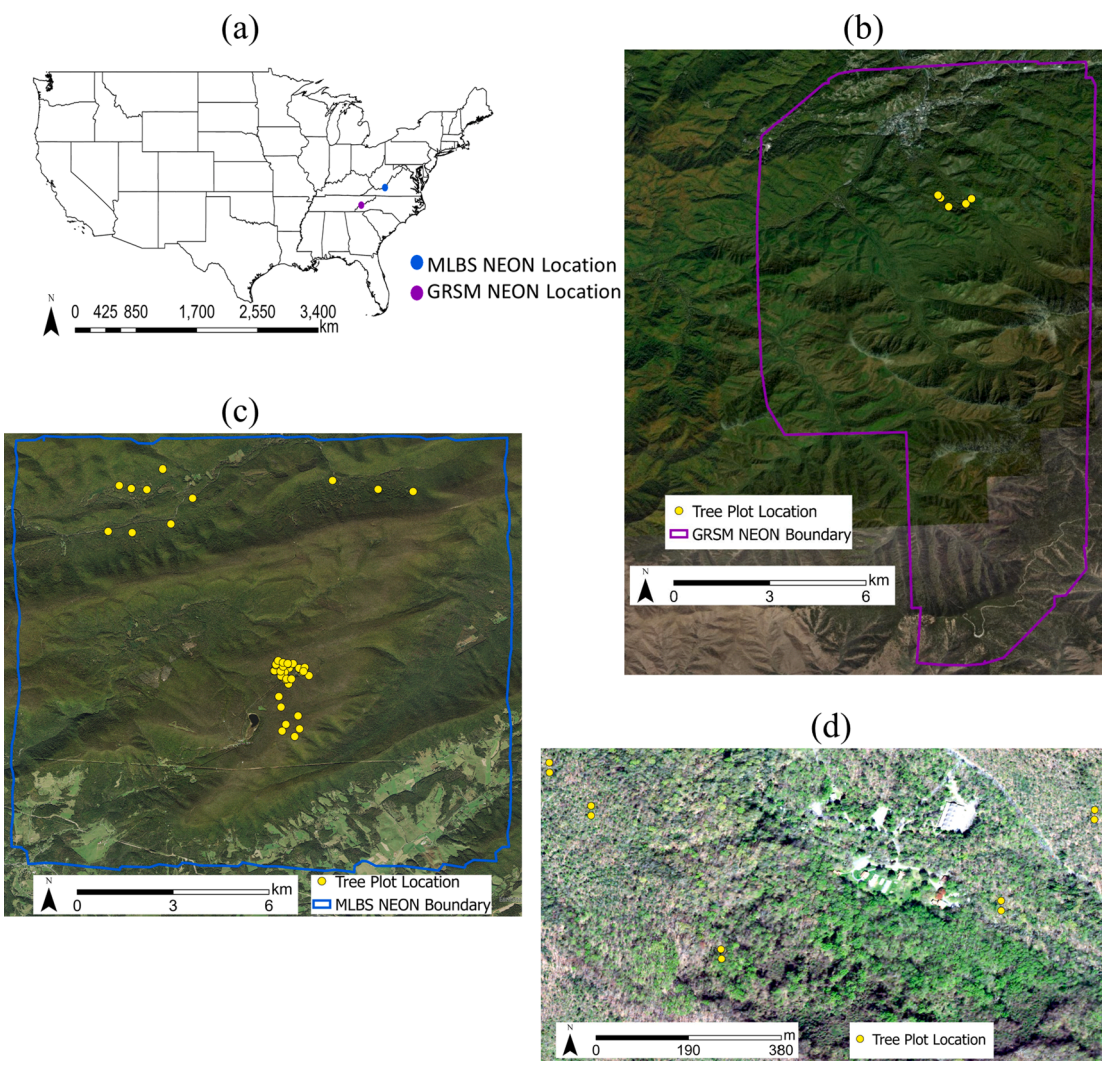

Fig. 1. Study site maps: (a) Overview map showing general location of MLBS and GRSM; (b) NEON GRSM in Tennessee, USA; (c) NEON MLBS site in Virginia, USA; (d) Zoom in on GRSM Twin Creeks Site where the ten tree plots (yellow dots) are located.

Further information about data quality efforts for woody structure measurements can be found in the NEON technical documents NEON.DOC.000914, NEON.DP1.10098 and NEON.DP1.10045. These field measurements can be found in the 'Woody plant vegetation structure' NEON product. From MLBS and GRSM, NEON has 52 tree plots and 10 tree plots, respectively, of 400 m^2 (0.04 ha). All plots from each study site were utilized in this study. See Table 1 for summary of tree measurements and Fig. 2 for distribution of each study site and combined datasets. In addition to the NEON measurements, we calculated mean dominant height (MDH) as the average height of the four tallest trees in each plot. The NEON tree data used in this study is plot location, height and species. NEON tree plot extent points were also downloaded.

The 2018 woody vegetation structure data was acquired through the NEON application programming interface (API). The vegetation "mapping and tagging" file was joined to the apparent individual tree file by using "individualID", "namedLocation", "domainID", "siteID" and "plotID" by using the NEON package. Quality control and assurance of tree data was done manually by communicating with NEON on which tree measurements were most up to date. The trees were then allocated to plots by their subplot ID. A python script was written to calculate average height and MDH for each plot. MDH was calculated by averaging the heights of the four tallest trees in each plot. The code also assigned each plot a label of single species, mixed deciduous, mixed coniferous or mixed both, based on the assigned NEON species and genus identification.

2.2.2. Remotely sensed data

NEON collected lidar data with approximately 4 points per square meter, with each point having up to 5 returns (NEON, 2020b). All lidar data used for this study were collected during May 2018 with an Optech Gemini sensor (Optech, Vaughan, Ontario, Canada). The NEON digital elevation model of 1 m spatial resolution was used for normalization of the lidar data (NEON, 2020c). This DEM was created by NEON based on their lidar data.

The 2018 NAIP imagery for Virginia and Tennessee were collected between 4 August and 18 December 2018. Specifically, the MLBS images were collected on 19 October 2018, while the GRSM images were collected on 30 October 2018. Multiple sensors were used, including serial numbers 10510, 10515, 10522, 10541, 10542, 10548, 10552 from Leica ADS-100 to collect data on four bands (blue: 435 nm to 495 nm; green: 525 nm to 585 nm; red: 619 nm to 651 nm; near infrared: 808 nm to 882 nm). A sampling distance of 0.4 m was achieved from 30% side overlap, and with a horizontal positional accuracy of +/- 6 m to true ground. To create a mosaic, autocorrelation algorithms were used to identify image tie points. More information about the metadata can be found in the following sources (OCM Partners, 2022; Ritz et al., 2021; USDA, 2011).

NAIP point clouds and DSMs for Virginia and Tennessee were purchased by the USFS as buy-up options through the NAIP. Vendors were awarded contracts to post-process the approximately 60 cm resolution stereo imagery routinely collected by NAIP into point clouds and then used these point clouds to create DSMs (NAIP, 2018). Point clouds were generated for each state using the airborne digital sensor (ADS) 100 imagery and Leica XPro SGM Module. The point clouds were delivered in LAZ 1.4 format with accompanying color infrared and RGB values encoded. Vendors also delivered DSMs at four times the collection density resulting in approximately 10 m raster surfaces. The orthorectified NAIP imagery, point clouds and DSM data are public domain, provided by the USDA Farm Service Agency. A 3DEP USGS 1 m resolution DEM was used for normalization of the NAIP point clouds (USGS, 2017) to emulate the data that a potential end user might have access to. This DEM was created by USGS 3DEP based on their lidar data. Please refer to Table 2 for a summary of all initial remotely sensed data that was used in this study.

Table 1
Summary of field measurements.

Measurement	MLBS	GRSM	Total
Number of plots	52	10	62
Mean height (m)	15.0	23.3	15.0
Average MDH (m)	21.2	23.5	21.5
Mean diameter (cm)	23.3	23.3	23.3
Mean basal area (m^2/ha)	1.5	0.8	1.5
Percent deciduous (%)	96	87	94
Number of species	27	23	39
Percent of trees measured (%)	97	97	97

2.3. Preprocessing remotely sensed data

The overall goal of these methods is to normalize the DSM, lidar and DAP point clouds in order to calculate plot heights. Processing and analysis were done using ArcGIS Pro, version 2.5.5 (ESRI, Redlands, CA, USA), USFS FUSION, version 4.00 (Corvallis, OR, USA) (McGaughey, 2009) and CloudCompare, version 2.11 (https://www.danielgm.net/cc/). First, DEMs were acquired for both datasets. The NEON DEM was used with the lidar data while a USGS DEM was used with the DAP data. Two different DEMs were used to simulate a user that could potentially utilize the DAP data with a DEM to calculate heights on their own land of interest. Since USFS FUSION requires DEM files to be in 'DTM' format, both DEMs were converted to ASCII files within ArcGIS Pro, and then were converted to.DTM files within USFS FUSION (ASCII2DTM). The dtm files were then merged (MergeDTM, USFS FUSION).

The next step was to create shapefiles of the measured plots with the same coordinate system and extents as the DEMs. The NEON plot corner points were downloaded and clipped to only include MLBS and GRSM points. These points were then further clipped to only include plot corner points that surround trees that NEON is actively monitoring. The Aggregate Points tool within ArcGIS Pro was then used to create individual polygons (Aggregate Points, ArcGIS Pro). These polygons were merged into two shapefiles to ensure the projection information was the same as the two DEMs. The extents were calculated for each plot and saved in the attribute table using the Add Geometry Attributes tool in ArcGIS Pro. The respective shapefiles were then used to clip the NEON DEM and USGS DEM using (clipDTM, USFS FUSION).

The raster domain tool in ArcGIS Pro was used to create a polygon of the NEON boundary extents. This polygon was used to select which NAIP tiles were needed. The individual NAIP las files were merged as well as the individual NEON LAS files. The raster domain polygon was used to clip the merged NAIP LAS file to the exact NEON boundary extents. This greatly helped reduce the NAIP LAS file size allowing for faster processing. For final quality control, CloudCompare was used to remove any outliers within the point clouds. The point clouds were then to simultaneously clipped, based on the calculated plot extent, and normalized, based on the clipped DEMs (clipData, USFS FUSION). Similarly, the NAIP DSM was clipped using the NEON plot shapefile and subtracted from the USGS DEM, resulting in a CHM for each plot.

Percentile heights and other statistical metrics were calculated for both the lidar and NAIP DAP point clouds (CloudMetrics, USFS FUSION). An overview of these steps can be seen in Fig. 3.

2.4. Statistical analysis

Following the well-established approach of estimating vegetation heights from lidar, regression was used for statistical analysis (Michez et al., 2020; Mielcarek et al., 2020; Pitt et al., 2014; Strunk et al., 2019, 2020). GeoDa (v. 1.18; (Anselin et al., 2021)) was used to assess the possible presence of global spatial autocorrelation using Moran's Index (Cliff and Ord, 1981; Moran, 1948). The dependent variable (MDH) and all three tested independent variables (the CHM derived from the NAIP DSM and the 90th percentile of heights from both the lidar and NAIP point clouds) exhibited significant spatial autocorrelation. For the point

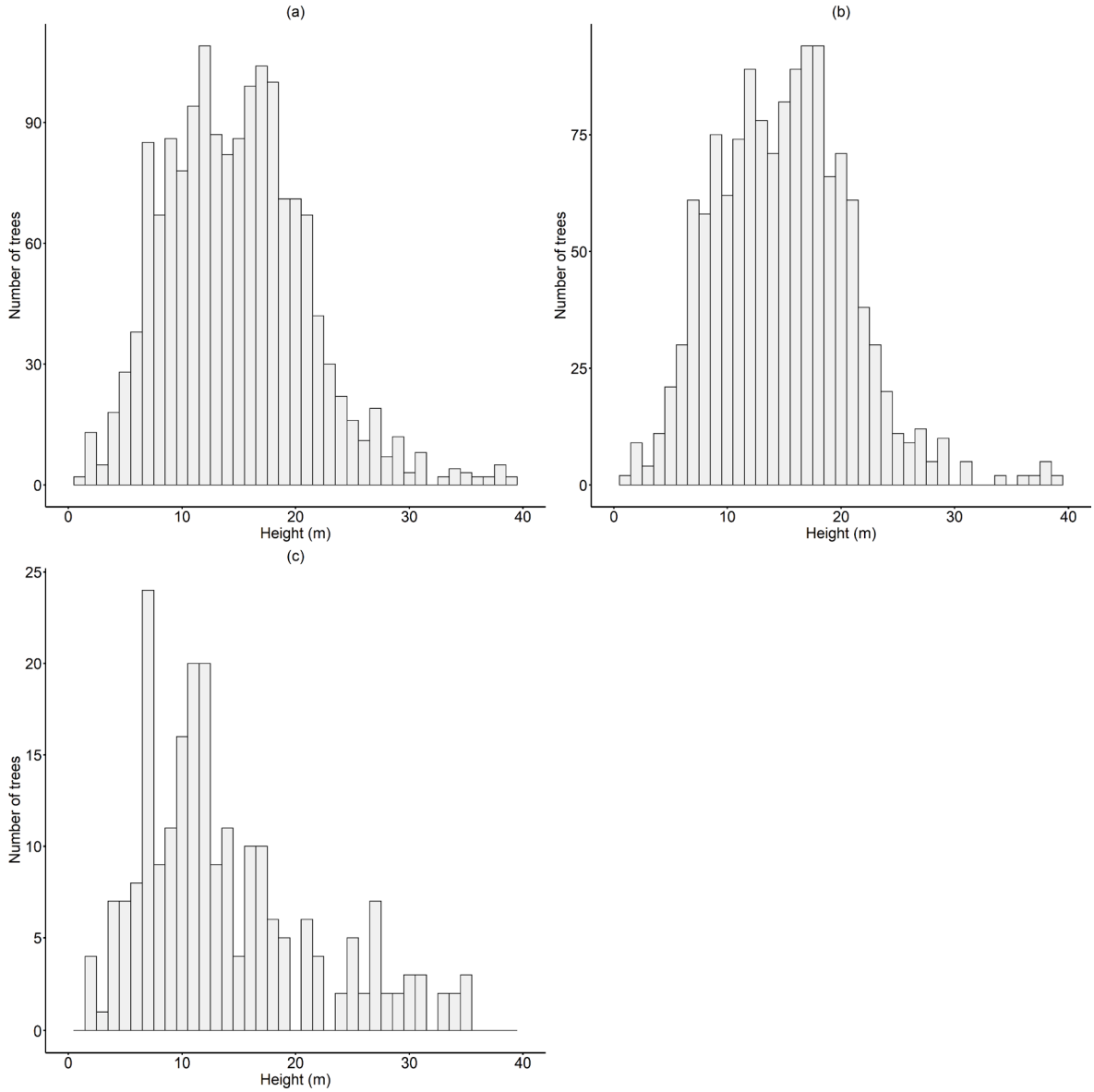

Fig. 2. Histograms show distributions of heights for each site and combined: (a) Histogram for all measured tree heights; (b) Histogram for MLBS measured tree heights; (c) Histogram for GRSM measured tree heights.

Table 2
Summary of initial remotely sensed data. All data, except for the USGS data, was collected in 2018.

Data Item	Type	Resolution (m)	Point density (points/ m^2)	Referred to in text	Raster source data	Source
Lidar	Point cloud	NA	22	Lidar	NA	NEON
DAP	Point cloud	NA	3	DAP	NA	NAIP
DSM	Raster	10	NA	DSM	NAIP DAP	NAIP
DEM	Raster	1	NA	DEM	NEON Lidar	NEON
DEM	Raster	1	NA	DEM	USGS Lidar	USGS

cloud data, it was decided to focus on the 90th percentile as the predictive variable since it is commonly used in research and industry (Mielcarek et al., 2020; Strunk et al., 2020).

An inverse distance weights matrix was created using the GeoDa weights manager using the default bandwidth (for this dataset) of 1,167 m, the minimum distance ensuring each plot had at least one neighboring plot. Classic ordinary least squares regression was performed in GeoDa using the inverse distance weights matrix for all three simple regressions (MDH vs. the NAIP 90th percentile height, MDH vs. the lidar 90th percentile height, and MDH vs. the CHM height derived from the NAIP DSM). The residuals of all regressions had significant Moran's Indexes. Robust Lagrange multiplier test diagnostics (Anselin, 1988) revealed error dependence but lack of spatial lag in the dependent variable (MDH) in all three models. Given the residuals in all three models were homoscedastic and normally distributed, the maximum likelihood spatial error model in GeoDa (Anselin, 2021; Anselin and Rey, 2014) was used to develop all three final models, eliminating spatial dependence in the residuals by adding on a spatial error term represented by λ.

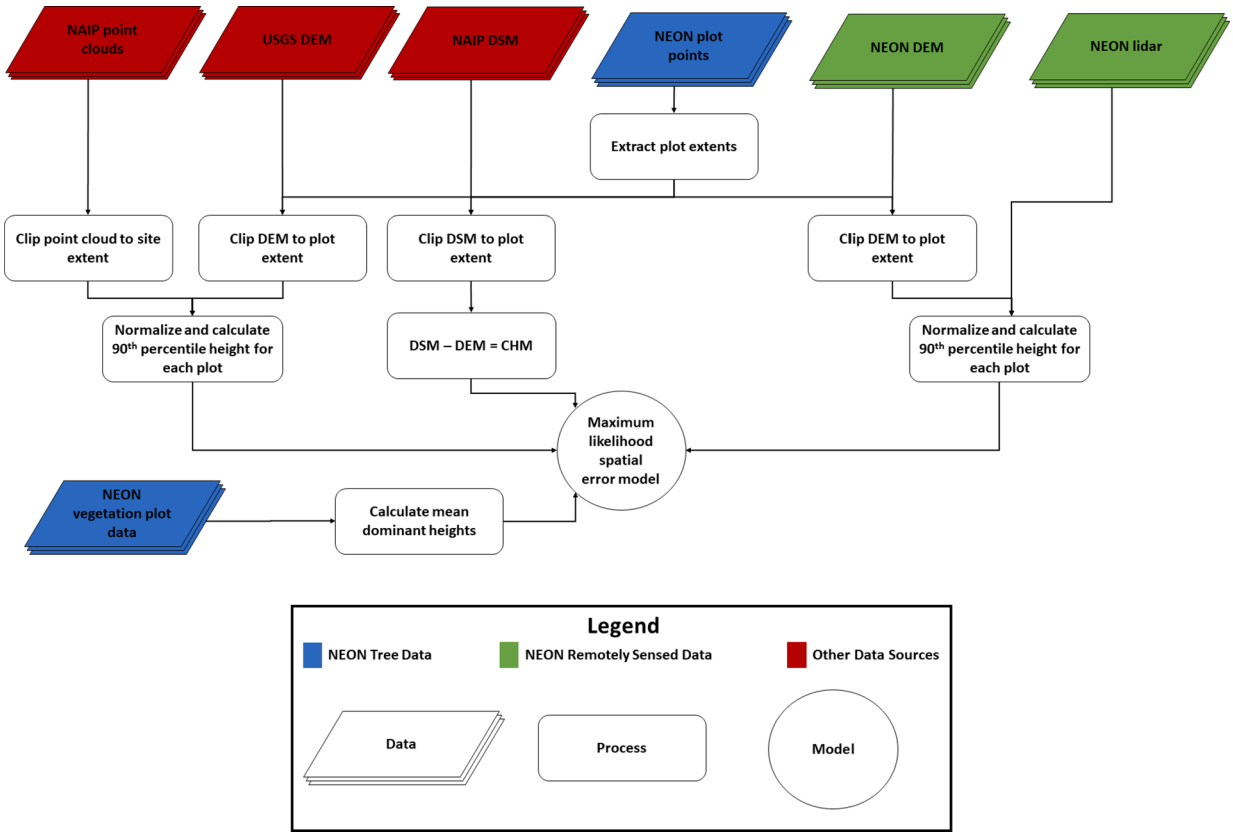

Fig. 3. Data processing flowchart.

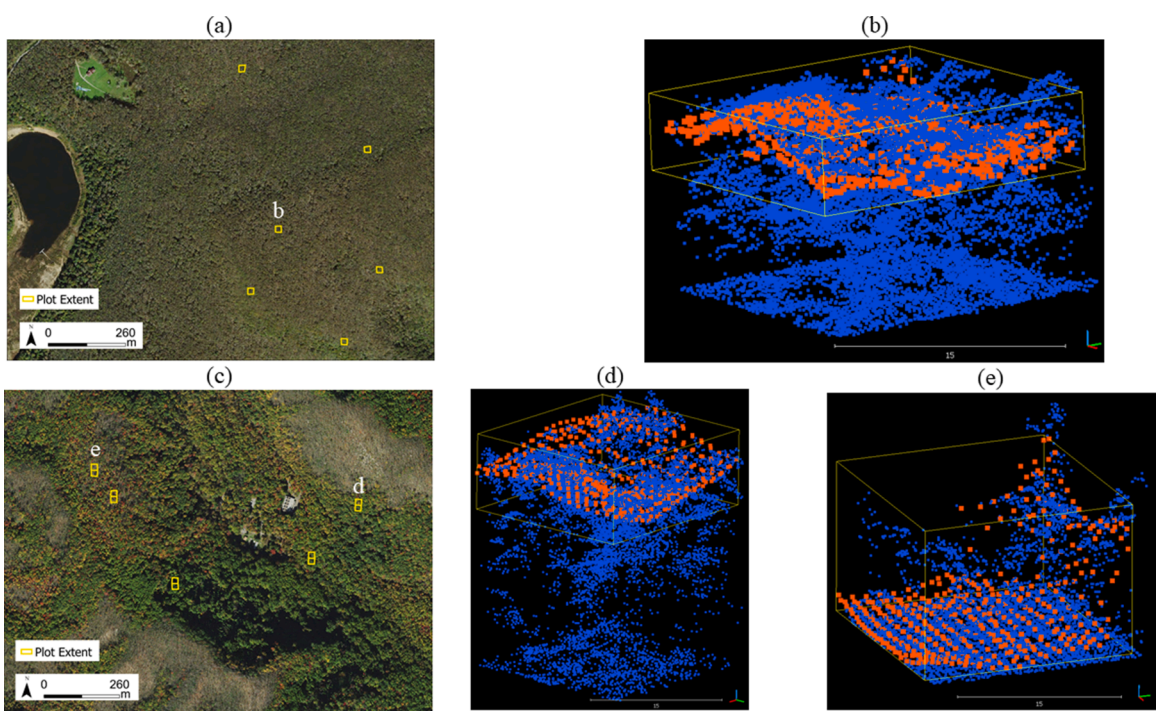

Fig. 4. Point cloud visualization, comparing DAP (orange) to lidar (blue) with the DAP extent outlined in yellow: (a) MLBS map showing 6 of the 52 tree plots with one labeled plot; (b) labeled plot from Fig. 4a showing DAP and lidar point clouds. This demonstrates the typical full canopy found at MLBS; (c) GRSM map showing all 10 tree plots with two labeled plots; (d) labeled plot from Fig. 4c showing DAP and lidar point clouds This is how most of the plot point cloud data at GRSM appears despite the 2016 wildfire; (e) labeled plot from Fig. 4c showing DAP and lidar point clouds. This plot and the plot directly below were the two most thinned plots due to the 2016 wildfire.

Coefficient of determinations (R^2) and the standard error of the estimate, also known as standard error (*SE*), were calculated for all the metrics. For this study the *SE* is described by Equation (1),

$$SE = \sqrt{\frac{\sum_{i=1}^{n}(y_i - \widehat{y}_i)^2}{n - df}} \quad (1)$$

where n is number of plots, i is a specific plot, y_i is the measured MDH of a specific plot, $\widehat{y}_i$ is the predicted MDH of a specific plot, and df is degrees of freedom.

2.5. Mapping the predictive model across the sites

The resulting predictive model for the NAIP 90th percentile heights was used to create a 10 m resolution raster of mean dominant height for each study site. This resolution was chosen to closely match the field plots, and to be more comparable with the NAIP DSM 10 m resolution product. The raster calculator in ArcGIS Pro was used to create the rasters by feeding the NAIP 90th percentile heights into the linear regression model.

3. Results

3.1. Visualization

Visualization of the normalized point clouds shows both remotely sensed datasets generally agree on mid to upper canopy heights (Fig. 4). As expected, the lidar dataset (blue) was able to easily detect the ground with the lowest points stopping at a flat surface. Additionally, from Fig. 4, DAP point clouds (orange) somewhat miss the very top of canopy and are unable to account for heights at mid and understory levels. Fig. 4e shows one of the GRSM plots that was affected by the 2016 wildfire, in which case the DAP point clouds were able to detect the ground.

3.2. NAIP DSM results

For the CHM sourced from the NAIP DSM, a strong linear trend with a slight overestimation can be observed (Fig. 5). A CHM raster with 10 m resolution was mapped over each study area (Fig. 6). This CHM raster is the result of subtracting the NAIP DSM from the USGS DEM. Further inspection of the resulting CHM shows that there are some areas with excessive heights of greater than 50 m in the GRSM site (Fig. 7). This is likely due to shadowing from steep terrain.

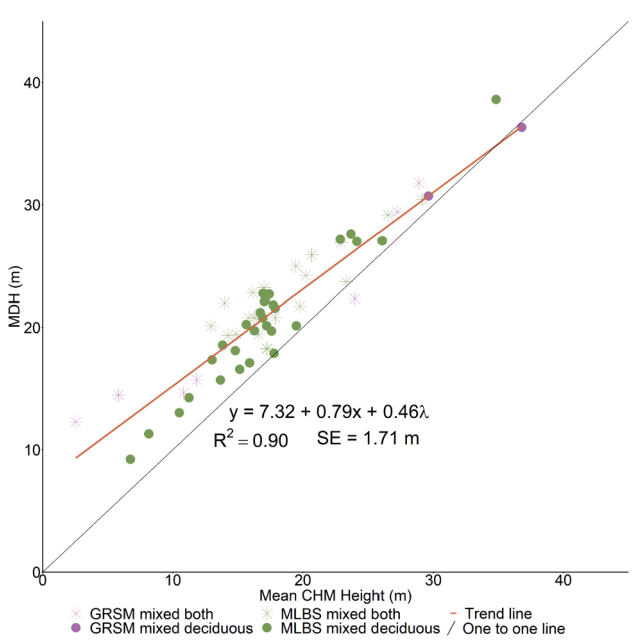

Fig. 5. MDH plotted against mean plot CHM height sourced from the 10 m NAIP DSM product. The black line is the one to one line. The trend line is the regression line without the spatial error term since the spatial error term is not constant.

3.3. NAIP point cloud results

Results from Fig. 8 show that there is a tight one-to-one linear trend between the two 90th percentile height remotely sensed datasets. Results from linear regression between the two MDH models and the 90th percentile height datasets resulted with lidar slightly outperforming NAIP point clouds with regard to *SE* and R^2 values (Fig. 9). The faded points indicate plots found at GRSM. An MDH raster with 10 m resolution was mapped over each study area (Fig. 10). This raster is the result of applying the models in Fig. 9 to a 90th percentile height raster.

The mixed deciduous and coniferous plots did not have any apparent clustering along the one-to-one line. Their general spread throughout the trendline may occur since while these plots did include coniferous trees, the plots were still dominated by deciduous trees. The NAIP point clouds had a slightly higher *SE*, but generally agreed with the lidar 90th percentile heights. When comparing all three models to each other, the lidar model nearly outperforms the DSM and NAIP model according to all the summary statistics shown in Table 3.

4. Discussion

The NAIP CHM derived from the NAIP DSM is of particular interest since it requires the least processing time for the end user. Note that the stars in Figs. 5, 6 and 7 indicate that the plot had both deciduous and coniferous trees while the solid points only had deciduous trees. Their relatively even dispersion shows that the presence of coniferous trees does not skew the data. Additionally, there was no clear bias in regard to tree plots from specific sites, thus showing that the observed trends do not clearly change between our study sites. Our results comparing DAP DSMs to plot tree heights are in agreement with other studies (Granholm et al., 2015; Mielcarek et al., 2020; Straub and Stepper, 2016). Additionally, the two study sites have relatively even distribution across the trendline showing that the model is adequate for both study sites. Although the DSM model did not perform as well as the point cloud models (lidar and NAIP models), it still performed relatively well, with most of the summary statistics comparable to the other two models (Table 3). Another important aspect to note about this study, is that despite the utilization of two different DEMs, the statistics are not in too much disagreement (Table 3), but could account for the minor disparities that are present.

The NAIP DAP point clouds' inability to consistently account for the very tops of trees is a common DAP limitation, which leads to a smooth canopy surface (Michez et al., 2020; Strunk et al., 2020; Xu et al., 2020; Yu et al., 2015). Our results showing that NAIP DAP point clouds are unable to detect the ground unless a consistent gap occurs, such as the plot affected by the wildfire in Fig. 4e, is also a common limitation for DAP point clouds (Strunk et al., 2020). Additionally, we compared 90th percentile heights of NAIP DAP point clouds and lidar to each other (Fig. 8). Similar trends are observed that were also seen in Fig. 5, including relatively even dispersal of each type of plot with regard to study site location and plot tree type.

To align with previous studies and industry practices, we only graphically compared the 90th percentile from both remotely sensed datasets to MDH (Fig. 9). The calculated statistics between lidar and NAIP DAP point clouds are very similar with NAIP DAP point clouds being slightly less accurate (Table 3 and Fig. 9). A number of other studies concluded with similar results that lidar slightly outperformed DAP (Järnstedt et al., 2012; Nurminen et al., 2013; Pearse et al., 2018; Strunk et al., 2020; Vastaranta et al., 2013; White et al., 2015; Xu et al.,

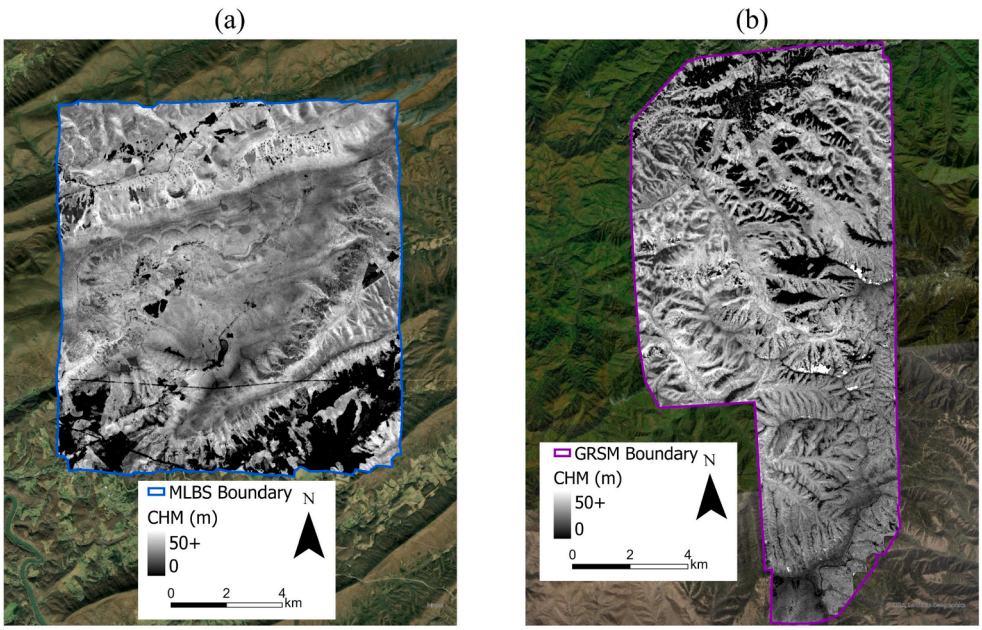

Fig. 6. CHM raster (10 m resolution) derived from the NAIP DSM for both study areas: (a) CHM over MLBS derived from the NAIP DSM; (b) CHM over GRSM derived from the NAIP DSM.

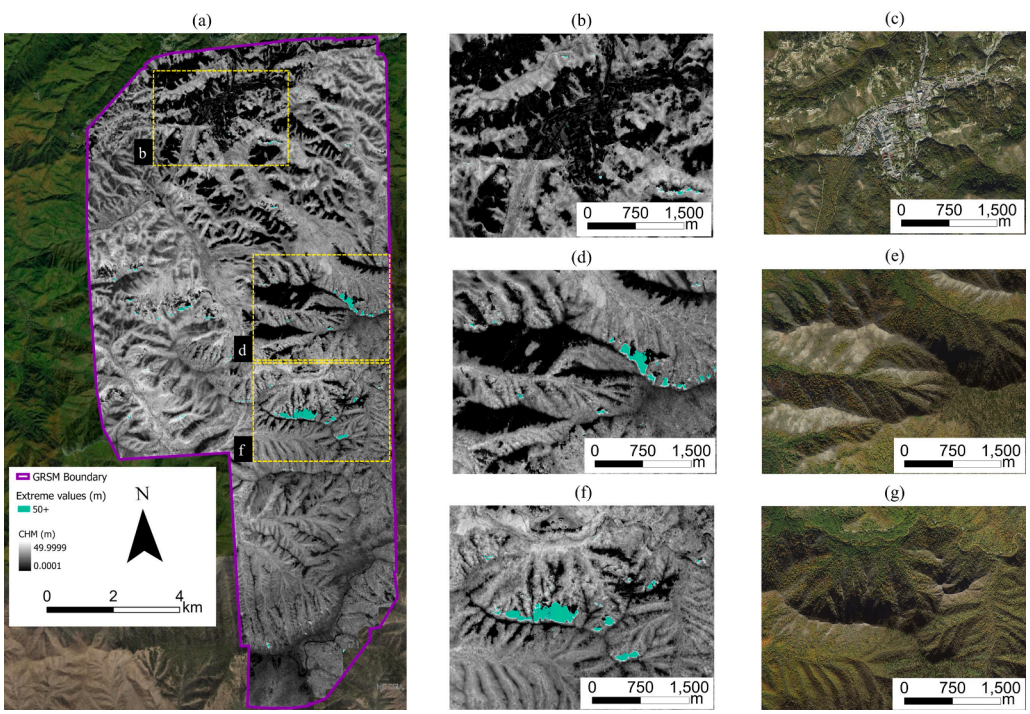

Fig. 7. CHM raster (10 m resolution) derived from the NAIP DSM for the GRSM site, with the cyan color indicating where excessive heights occur that are greater than 50 m (a). From further inspection of the raster (b, d and f), shadowing seen in panels c, e and f seems to have caused these excessive heights to occur. The MLBS site did not have these issues.

2020; Yu et al., 2015).

Lastly, MDH rasters were developed for both study sites using the linear model developed from NAIP DAP 90th percentile heights and MDH based on height (Fig. 10). It should be pointed out that where high elevation relief occurs, such as steep slopes and ravines, the NAIP DAP point clouds missed patches of trees. This same occurrence was noted by (Michez et al., 2020) in their regional DAP point cloud versus lidar study. This only occurred for the GRSM site, which can be seen in Fig. 6b and 10b where white patches occur tapering off of peaks, and is further highlighted by the cyan color in Fig. 7. These problematic locations did not occur in the tree plots used for linear regression model development, thus there is no effect on the models previously presented. For future use, treeless patches could be filtered out. One likely explanation for this issue is that not enough overlap occurred in these critical areas. It is also evident that GRSM has more dramatic occurrence of elevation change and thus steep slopes occurring within a short distance, which could also be a contributing factor. Upon visual inspection of the NAIP imagery, these problematic patches occurred in sloped areas that were often

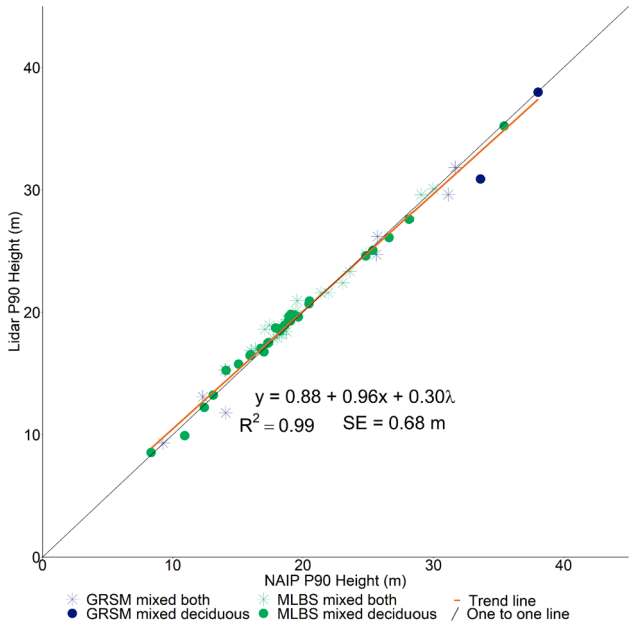

Fig. 8. 90th percentile lidar heights compared to 90th percentile DAP point cloud heights. The black line is the one-to-one line. The trend line is the regression line without the spatial error term since the spatial error term is not constant.

shadowed (Fig. 7). Shadowing has been found to lead to DAP errors (Halbritter, 1999; Iqbal et al., 2018; Rahlf et al., 2017, 2014; White et al., 2018). Plots with high complexity are more likely to have erroneous DAP data, which has been seen for tree gaps and complex canopy structures (Mielcarek et al., 2020; Ritz et al., 2021; White et al., 2018). Additionally, DAP point clouds have been found to have difficulty with capturing canopy data for young and sparse plots, probably due to shadowing and gaps from row plantation plantings (Næsset, 2002; Ritz et al., 2021; Yu et al., 2015). While these issues were not found in our tree plots, gaps, shadowing and steep slopes seem to be some of the main limitations of DAP data which should be addressed in future research.

One likely reason for our results showing such high R^2 values is that this study was conducted over forests with dense canopies due to the dominant deciduous trees. These deciduous forests often consist of trees with leaves that have high surface area that essentially closes the canopy of many gaps typically found in boreal and evergreen forests (Halbritter, 1996; Næsset, 2002). It should be noted though that the NAIP imagery used in this study was collected at the end of October (19 October for MLBS and 30 October for GRSM) with potential leaf-off conditions occurring at this time. Despite this, our results demonstrate NAIP's comparable ability to measure MDH for deciduous forests.

Similar comparison studies utilizing NAIP DAP point clouds have been conducted in Washington (Strunk et al., 2019, 2020), where the latter shows that DAP resolution (7.5 cm, 15 cm, 30 cm frame camera and 40 cm pushbroom NAIP) did not greatly alter the ability to measure forest attributes, which agrees with our study (60 cm pushbroom NAIP DAP) and a number of other studies that used non-NAIP DAP (Bohlin et al., 2012; Gobakken et al., 2015; Nurminen et al., 2013). Our study is the first NAIP DAP study conducted over deciduous forests in the southeastern region of the US and utilizes data from forests separated by over 325 km with minimal model bias towards one location. The overall success and the location of our study have far-reaching implications, confirming that largely deciduous forests are able to be measured using NAIP DAP point clouds and DSM.

Future work should include investigation of parameter sensitivity with regard to point cloud formation from pushbroom imagery along with determining minimum overlap needed to ensure continuous landscape representation in order to address previous stated limitations due

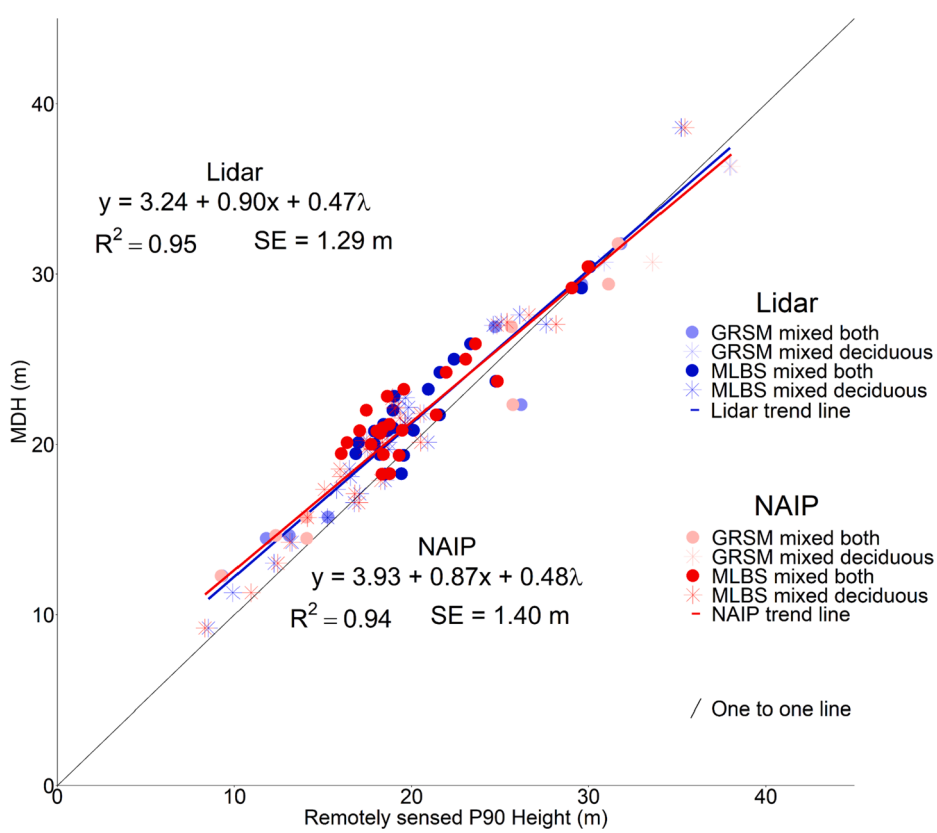

Fig. 9. Scatterplot of MDH against 90th percentile remotely sensed plot data. The faded data points are from GRSM. The black line is the one-to-one line. The trend lines are the regression lines without the spatial error term since the spatial error term is not constant.

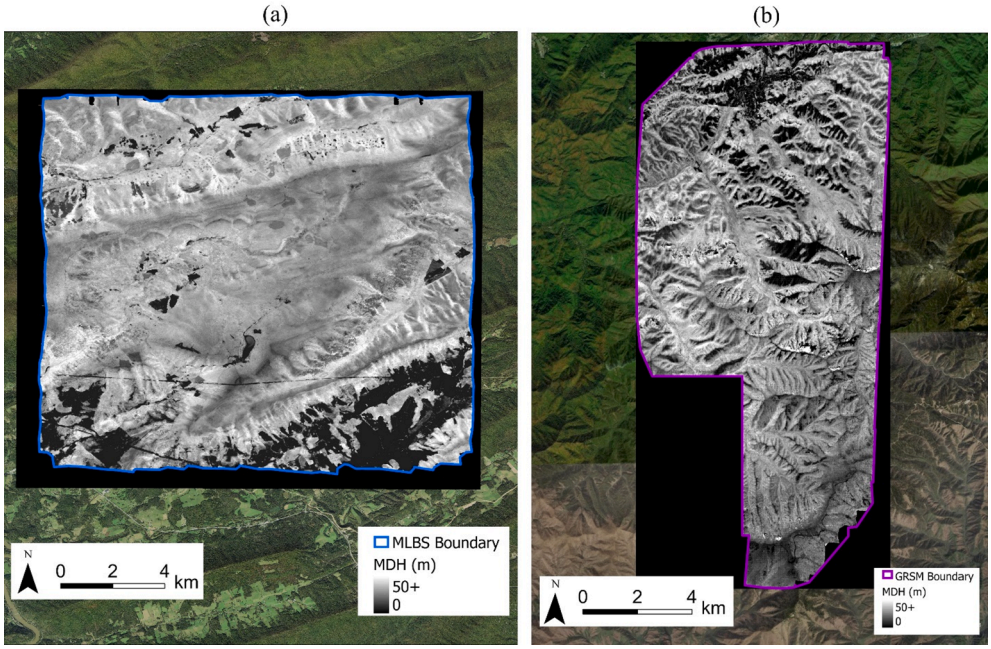

Fig. 10. MDH raster (10 m resolution) from the linear model applied to both study areas: (a) MDH over MLBS using the linear model developed from NAIP DAP 90th percentile; (b) MDH over GRSM using the linear model developed from NAIP DAP 90th percentile.

Table 3
Summary of model statistics.

	Input Data		Coefficient	*SE* for each variable (m)	R^2	*SE*(m)	Akaike Information Criterion	Log likelihood
DSM Model	CHM Derived from NAIP DSM	Constant	7.32	0.79	0.90	1.71	248.62	−122.31
		Remotely Sensed Height	0.79	0.04				
		λ	0.46	0.15				
NAIP Model	P90 from NAIP DAP point clouds	Constant	3.93	0.76	0.94	1.40	224.17	−110.08
		Remotely Sensed Height	0.87	0.03				
		λ	0.48	0.15				
Lidar Model	90P from NEON lidar point clouds	Constant	3.24	0.72	0.95	1.29	213.92	−104.96
		Remotely Sensed Height	0.90	0.03				
		λ	0.47	0.15				

to gaps, shadowing and steep slopes. These knowledge gaps are likely the main limitations to NAIP DAP currently known due to the patches seen in Figs. 6b, 7 and 10b, and also the complicated nature of photogrammetric processing (Goodbody et al., 2019; Iqbal et al., 2018; Strunk et al., 2020). In addition to parameter adjustment and overlap assessment, a combination of other data sources with NAIP DAP, such as from other remote sensing platforms (Kwong and Fung, 2020; St-Onge et al., 2008) or auxiliary information, like thinning status (Green et al., 2020) or slope (Michez et al., 2020), could be used for particularly problematic areas. Once these limitations are addressed, regional processing could begin with the potential of a national CHM. Multitemporal capabilities via NAIP and 3DEP would allow for forests to be accounted for at a national scale through time, with regard to improved comprehensive estimates of rejuvenation versus deforestation, carbon sequestration and wildfire impact.

5. Conclusions

For this study, 2018 NAIP DSM and DAP point cloud datasets were compared to 2018 NEON MLBS and GRSM lidar datasets and tree height field measurements. Heights were calculated by normalizing the point clouds with DEMs. The results showed a strong linear trend between the NAIP DSM and field measurements and the NAIP normalized DAP and the lidar normalized point clouds. From these results, it can be surmised that DSMs and DAP point clouds can be used to estimate MDH for forests, with similar acquisition parameters, terrain as well as similar forest characteristics, including canopy type, maturity and closure. Future research should focus on defining best practices for DAP collection, with regard to necessary overlap, and DAP point cloud formation. Once these limitations have been addressed, the potential for consistent multitemporal CHMs and estimation of mean dominant height through NAIP will be attainable.

Declaration of Competing Interest

The authors declare that they have no known competing financial interests or personal relationships that could have appeared to influence the work reported in this paper.

Acknowledgements

This work was supported by the Virginia Tech Interdisciplinary Graduate Education Program in Remote Sensing and the National Science Graduate Research Fellowship Program under Grant No.1840995.

The authors would like to acknowledge Margaret Cumberland (NEON Field Ecologist II) for her guidance on the NEON woody structure data. Special thanks to the university departments for ensuring access to resources during the COVID-19 pandemic.

References

Anselin, L., 2021. GeoDa Workbook. GeoDa Doc.

Anselin, L., 1988. Lagrange multiplier test diagnostics for spatial dependence and spatial heterogeneity. Geogr. Anal. 20, 1–17.

Anselin, L., Koschinsky, J., Li, X., 2021. GeoDa v. 1.18. GeoDa Introd. Spat. Data Sci.

Anselin, L., Rey, S.J., 2014. Modern spatial econometrics in practice: A guide to GeoDa, GeoDaSpace and PySAL. GeoDa Press LLC.

Basu, S., Ganguly, S., Nemani, R.R., Mukhopadhyay, S., Zhang, G., Milesi, C., Michaelis, A., Votava, P., Dubayah, R., Duncanson, L., 2015. A semiautomated probabilistic framework for tree-cover delineation from 1-m NAIP imagery using a high-performance computing architecture. IEEE Trans. Geosci. Remote Sens. 53, 5690–5708. https://doi.org/10.1109/TGRS.2015.2428197.

Bohlin, J., Wallerman, J., Fransson, J.E., 2012. Forest variable estimation using photogrammetric matching of digital aerial images in combination with a high-resolution DEM. Scand. J. For. Res. 27, 692–699. https://doi.org/10.1080/02827581.2012.686625.

Cliff, A.D., Ord, J.K., 1981. Spatial Processes: Models and Applications (Pion Limited). Taylor & Francis, London.

Davies, K.W., Petersen, S.L., Johnson, D.D., Davis, D.B., Madsen, M.D., Zvirzdin, D.L., Bates, J.D., 2010. Estimating juniper cover from National Agriculture Imagery Program (NAIP) imagery and evaluating relationships between potential cover and environmental variables. Rangel. Ecol. Manag. 63, 630–637. https://doi.org/10.2111/REM-D-09-00129.1.

Gobakken, T., Bollandsås, O.M., Næsset, E., 2015. Comparing biophysical forest characteristics estimated from photogrammetric matching of aerial images and airborne laser scanning data. Scand. J. For. Res. 30, 73–86. https://doi.org/10.1080/02827581.2014.961954.

Goodbody, T.R., Coops, N.C., White, J.C., 2019. Digital aerial photogrammetry for updating area-based forest inventories: a review of opportunities, challenges, and future directions. Curr. For. Rep. 5, 55–75. https://doi.org/10.1007/s40725-019-00087-2.

Gopalakrishnan, R., Kauffman, J.S., Fagan, M.E., Coulston, J.W., Thomas, V.A., Wynne, R.H., Fox, T.R., Quirino, V.F., 2019. Creating landscape-scale site index maps for the southeastern US is possible with airborne LiDAR and landsat imagery. Forests 10, 234. https://doi.org/10.3390/f10030234.

Granholm, A.-H., Olsson, H., Nilsson, M., Allard, A., Holmgren, J., 2015. The potential of digital surface models based on aerial images for automated vegetation mapping. Int. J. Remote Sens. 36, 1855–1870. https://doi.org/10.1080/01431161.2015.1029094.

Green, P.C., Burkhart, H.E., Coulston, J.W., Radtke, P.J., 2020. A novel application of small area estimation in loblolly pine forest inventory. For. Int. J. For. Res. 93, 444–457. https://doi.org/10.1093/forestry/cpz073.

Halbritter, K., 1999. Remote sensing for quantifying structural diversity in forests for forest biodiversity assessment. In: Forests in Focus: Proceedings Forum, Biodiversity-Treasures in the World's Forests, 3-7 July 1998. Alfred Toepfer Foundation, pp. 185–192.

Halbritter, K., 1996. Steps towards a forest biodiversity information system: Quantifying forest biodiversity by photogrammetry and remote sensing methodology. In: Proceedings of International Symposium, Application of Remote Sensing in Forestry, Zvolen, Slovakia, pp. 119–133.

Hartfield, K.A., Landau, K.I., Van Leeuwen, W.J., 2011. Fusion of high resolution aerial multispectral and LiDAR data: Land cover in the context of urban mosquito habitat. Remote Sens. 3, 2364–2383. https://doi.org/10.3390/rs3112364.

Hogland, J., Anderson, N., St Peter, J., Drake, J., Medley, P., 2018. Mapping forest characteristics at fine resolution across large landscapes of the southeastern United States using NAIP imagery and FIA field plot data. ISPRS Int. J. Geo-Inf. 7, 140. https://doi.org/10.3390/ijgi7040140.

Immitzer, M., Stepper, C., Böck, S., Straub, C., Atzberger, C., 2016. Use of WorldView-2 stereo imagery and National Forest Inventory data for wall-to-wall mapping of growing stock. For. Ecol. Manag. 359, 232–246. https://doi.org/10.1016/j.foreco.2015.10.018.

Iqbal, I.A., Osborn, J., Stone, C., Lucieer, A., Dell, M., McCoull, C., 2018. Evaluating the robustness of point clouds from small format aerial photography over a Pinus radiata plantation. Aust. For. 81, 162–176. https://doi.org/10.1080/00049158.2018.1482799.

Järnstedt, J., Pekkarinen, A., Tuominen, S., Ginzler, C., Holopainen, M., Viitala, R., 2012. Forest variable estimation using a high-resolution digital surface model. ISPRS J. Photogramm. Remote Sens. 74, 78–84. https://doi.org/10.1016/j.isprsjprs.2012.08.006.

Jenkins, M.A., 2007. Vegetation communities of Great Smoky Mountains National Park. Southeast. Nat. 6, 35–56. https://doi.org/10.1656/1528-7092(2007)6[35:VCOGSM]2.0.CO;2.

Kwong, I.H., Fung, T., 2020. Tree height mapping and crown delineation using LiDAR, large format aerial photographs, and unmanned aerial vehicle photogrammetry in subtropical urban forest. Int. J. Remote Sens. 41, 5228–5256. https://doi.org/10.1080/01431161.2020.1731002.

Liknes, G.C., Perry, C.H., Meneguzzo, D.M., 2010. Assessing tree cover in agricultural landscapes using high-resolution aerial imagery. J. Terr. Obs. 2, 38–55.

Lukas, V., Baez, V., 2021. 3D Elevation Program—Federal best practices: U.S. Geological Survey Fact Sheet 2020–3062, Fact Sheet. US Geological Survey, Reston, VA, USA.

Ma, Q., Su, Y., Guo, Q., 2017. Comparison of canopy cover estimations from airborne LiDAR, aerial imagery, and satellite imagery. IEEE J Sel. Top. Appl. Earth Obs. Remote Sens. 10, 4225–4236. https://doi.org/10.1109/JSTARS.2017.2711482.

Maxwell, A., Strager, M., Warner, T., Zégre, N., Yuill, C., 2014. Comparison of NAIP orthophotography and RapidEye satellite imagery for mapping of mining and mine reclamation. GIScience Remote Sens. 51, 301–320. https://doi.org/10.1080/15481603.2014.912874.

McGaughey, R.J., 2009. FUSION/LDV: Software for LIDAR data analysis and visualization. US Dep. Agric. For. Serv. Pac. Northwest Res. Stn, Seattle WA USA, p. 123.

Michez, A., Huylenbroeck, L., Bolyn, C., Latte, N., Bauwens, S., Lejeune, P., 2020. Can regional aerial images from orthophoto surveys produce high quality photogrammetric canopy height model? A single tree approach in Western Europe. Int. J. Appl. Earth Obs. Geoinformation 92, 102190. https://doi.org/10.1016/j.jag.2020.102190.

Mielcarek, M., Kamińska, A., Stereńczak, K., 2020. Digital aerial photogrammetry (DAP) and airborne laser scanning (ALS) as sources of information about tree height: comparisons of the accuracy of remote sensing methods for tree height estimation. Remote Sens. 12, 1808. https://doi.org/10.3390/rs12111808.

Mills, H.H., 1988. Surficial geology and geomorphology of the Mountain Lake area, Giles County, Virginia, including sedimentological studies of colluvium and boulder streams (USGS Report No. 1469), Professional Paper. USGS. 10.3133/pp1469.

Moran, P.A., 1948. The interpretation of statistical maps. J. R. Stat. Soc. Ser. B Methodol. 10, 243–251.

Næsset, E., 2002. Determination of mean tree height of forest stands by digital photogrammetry. Scand. J. For. Res. 17, 446–459. https://doi.org/10.1080/028275802320435469.

NAIP, 2018. National Agriculture Imagery Program (NAIP) Digital Aerial Photography 3D point cloud product.

Navarro, J.A., Tomé, J.L., Marino, E., Guillén-Climent, M.L., Fernández-Landa, A., 2020. Assessing the transferability of airborne laser scanning and digital aerial photogrammetry derived growing stock volume models. Int. J. Appl. Earth Obs. Geoinformation 91, 102135.

NEON, N.E.O.N., 2020a. Woody plant vegetation structure, RELEASE-2020 (DP1.10098.001). 10.48443/e3qn-xw47.

NEON, N.E.O.N., 2020b. Discrete return LiDAR point cloud, RELEASE-2021 (DP1.30003.001). 10.48443/6e8k-3343.

NEON, N.E.O.N., 2020c. Elevation - LiDAR, RELEASE-2020 (DP3.30024.001). 10.48443/917d-g459.

Nurminen, K., Karjalainen, M., Yu, X., Hyyppä, J., Honkavaara, E., 2013. Performance of dense digital surface models based on image matching in the estimation of plot-level forest variables. ISPRS J. Photogramm. Remote Sens. 83, 104–115. https://doi.org/10.1016/j.isprsjprs.2013.06.005.

OCM Partners, 2022. 2018 Virginia NAIP Digital Ortho Photo Imagery.

Pearse, G.D., Dash, J.P., Persson, H.J., Watt, M.S., 2018. Comparison of high-density LiDAR and satellite photogrammetry for forest inventory. ISPRS J. Photogramm. Remote Sens. 142, 257–267. https://doi.org/10.1016/j.isprsjprs.2018.06.006.

Pitt, D.G., Woods, M., Penner, M., 2014. A comparison of point clouds derived from stereo imagery and airborne laser scanning for the area-based estimation of forest inventory attributes in boreal Ontario. Can. J. Remote Sens. 40, 214–232. https://doi.org/10.1080/07038992.2014.958420.

Price, B., Waser, L.T., Wang, Z., Marty, M., Ginzler, C., Zellweger, F., 2020. Predicting biomass dynamics at the national extent from digital aerial photogrammetry. Int. J. Appl. Earth Obs. Geoinformation 90, 102116. https://doi.org/10.1016/j.jag.2020.102116.

Puliti, S., Ørka, H.O., Gobakken, T., Næsset, E., 2015. Inventory of small forest areas using an unmanned aerial system. Remote Sens. 7, 9632–9654. https://doi.org/10.3390/rs70809632.

Rahlf, J., Breidenbach, J., Solberg, S., Næsset, E., Astrup, R., 2017. Digital aerial photogrammetry can efficiently support large-area forest inventories in Norway. For. Int. J. For. Res. 90, 710–718. https://doi.org/10.1093/forestry/cpx027.

Rahlf, J., Breidenbach, J., Solberg, S., Næsset, E., Astrup, R., 2014. Comparison of four types of 3D data for timber volume estimation. Remote Sens. Environ. 155, 325–333. https://doi.org/10.1016/j.rse.2014.08.036.

Ritz, A., Thomas, V.A., Schroeder, T., Wynne, R.H., 2021. Assessing the utility of NAIP digital aerial photogrammetric point clouds for estimating canopy height of managed loblolly pine plantations in the southeastern United States (M.S. Thesis). Virginia Tech.

Samiappan, S., Hathcock, L., Turnage, G., McCraine, C., Pitchford, J., Moorhead, R., 2019. Remote sensing of wildfire using a small unmanned aerial system: post-fire mapping, vegetation recovery and damage analysis in grand bay, Mississippi/Alabama, USA. Drones 3, 43. https://doi.org/10.3390/drones3020043.

Schultz, A.P., Stanley, C.B., Gathright, T.M., Rader, E.K., Bartholomew, M.J., Lewis, S.E., Evans, N.H., 1986. Geologic Map of Giles County, Virginia.

Sharkey, M.J., 2001. The all taxa biological inventory of the Great Smoky Mountains National Park. Fla. Entomol. 556–564 https://doi.org/10.2307/3496388.

Southworth, S., Schultz, A., Denenny, D., 2004. Generalized geologic map of bedrock lithologies and surficial deposits in the Great Smoky Mountains National Park Region, Tennessee and North Carolina. US Geol. Surv. Open-File Rep. 2005, 1410.

St-Onge, B., Hu, Y., Vega, C., 2008. Mapping the height and above-ground biomass of a mixed forest using lidar and stereo IKONOS images. Int. J. Remote Sens. 29, 1277–1294. https://doi.org/10.1080/01431160701736505.

Straub, C., Stepper, C., 2016. Using digital aerial photogrammetry and the random forest approach to model forest inventory attributes in Beech-and Spruce-dominated

Central European Forests. PFG Photogramm. Fernerkund. Geoinformation 109–123. https://doi.org/10.1127/pfg/2016/0292.

Strunk, J., Packalen, P., Gould, P., Gatziolis, D., Maki, C., Andersen, H.-E., McGaughey, R.J., 2019. Large area forest yield estimation with pushbroom digital aerial photogrammetry. Forests 10, 397. https://doi.org/10.3390/f10050397.

Strunk, J.L., Gould, P.J., Packalen, P., Gatziolis, D., Greblowska, D., Maki, C., McGaughey, R.J., 2020. Evaluation of pushbroom DAP relative to frame camera DAP and lidar for forest modeling. Remote Sens. Environ. 237, 111535 https://doi.org/10.1016/j.rse.2019.111535.

USDA, 2011. NAIP Imagery [WWW Document]. URL https://www.fsa.usda.gov/programs-and-services/aerial-photography/imagery-programs/naip-imagery/.

USGS, U.S.G.S., 2017. 1 meter Digital Elevation Models (DEMs) - USGS National Map 3DEP Downloadable Data Collection.

Vastaranta, M., Niemi, M., Karjalainen, M., Peuhkurinen, J., Kankare, V., Hyyppä, J., Holopainen, M., 2014. Prediction of forest stand attributes using TerraSAR-X stereo imagery. Remote Sens. 6, 3227–3246. https://doi.org/10.3390/rs6043227.

Vastaranta, M., Wulder, M.A., White, J.C., Pekkarinen, A., Tuominen, S., Ginzler, C., Kankare, V., Holopainen, M., Hyyppä, J., Hyyppä, H., 2013. Airborne laser scanning and digital stereo imagery measures of forest structure: comparative results and implications to forest mapping and inventory update. Can. J. Remote Sens. 39, 382–395. https://doi.org/10.5589/m13-046.

White, J.C., Stepper, C., Tompalski, P., Coops, N.C., Wulder, M.A., 2015. Comparing ALS and image-based point cloud metrics and modelled forest inventory attributes in a complex coastal forest environment. Forests 6, 3704–3732. https://doi.org/10.3390/f6103704.

White, J.C., Tompalski, P., Coops, N.C., Wulder, M.A., 2018. Comparison of airborne laser scanning and digital stereo imagery for characterizing forest canopy gaps in coastal temperate rainforests. Remote Sens. Environ. 208, 1–14. https://doi.org/10.1016/j.rse.2018.02.002.

Wilbur, R.B., Wilbur, H.M., Peterson, N.J., 2021. Flora of the forest at Mountain Lake Biological Station, Giles County, Virginia. Castanea 85, 376–403. https://doi.org/10.2179/0008-7475.85.2.376.

Xu, Z., Ruan, H., Chen, H.Y., 2020. Comparison of stand characteristic parameters and biomass estimations from light detection and ranging and structure-from-motion point clouds. J. Appl. Remote Sens. 14, 022209 https://doi.org/10.1117/1.JRS.14.022209.

Yu, X., Hyyppä, J., Karjalainen, M., Nurminen, K., Karila, K., Vastaranta, M., Kankare, V., Kaartinen, H., Holopainen, M., Honkavaara, E., 2015. Comparison of laser and stereo optical, SAR and InSAR point clouds from air-and space-borne sources in the retrieval of forest inventory attributes. Remote Sens. 7, 15933–15954. https://doi.org/10.3390/rs71215809.